Research Square

Preprints are preliminary reports that have not undergone peer review.
They should not be considered conclusive, used to inform clinical practice,
or referenced by the media as validated information.

Thermodynamic Analysis of a Two-Stage Selective Carbothermic Reduction Process for Deep-Sea Polymetallic Nodules: Part I. Selective Recovery of Critical Battery Metals

Omid Marzoughi

om17@queensu.ca

Queen's University

Dulmini Hissalle

Queen's University

Christopher Pickles

Queen's University

Research Article

Keywords: Deep-sea polymetallic nodules, selective carbothermic reduction, critical battery metals, thermodynamic modelling, HSC Chemistry, equilibrium modelling

Posted Date: November 19th, 2026

DOI: https://doi.org/10.21203/rs.3.rs-11292096/v1

License: This work is licensed under a Creative Commons Attribution 4.0 International License.
Read Full License

Additional Declarations: No competing interests reported.

Thermodynamic Analysis of a Two-Stage Selective Carbothermic Reduction Process for Deep-Sea Polymetallic Nodules: Part I. Selective Recovery of Critical Battery Metals

O. Marzoughi, D. Hissalle, C. A. Pickles

Robert M. Buchan Department of Mining, Queen's University, Kingston,

Ontario, Canada, K7L 3N6

ABSTRACT

Deep-sea polymetallic nodules are a promising resource for critical metals, but their fine-grained mineralogy and complex Mn–Fe oxide matrix make conventional processing challenging. This study presents a thermodynamic analysis of the first stage of a proposed two-stage selective carbothermic process to recover Cu, Ni and Co as a Cu–Ni–Co–Fe alloy while suppressing manganese reduction. Equilibrium calculations were performed using the Equilibrium Composition module of HSC Chemistry® 7.1 for a representative nodule composition. The effects of temperature, carbon addition, total pressure, atmosphere and nodule composition on metal recoveries and alloy composition were evaluated. The results demonstrate a well-defined thermodynamic operating window in which Cu, Ni and Co can be selectively recovered with limited iron reduction while manganese remains predominantly in the oxide phase. The predicted reduction sequence and recovery trends were consistent with published experimental observations. The study establishes the thermodynamic basis for Stage I and provides a manganese-rich residue for subsequent high-temperature production of a ferromanganese–silicide alloy in Part II.

Keywords: Deep-sea polymetallic nodules; selective carbothermic reduction; critical battery metals; thermodynamic modelling; HSC Chemistry; equilibrium modelling.

1 Introduction

Polymetallic nodules are a promising source of critical metals and are found on the abyssal plains at depths of approximately 4,000–6,000 m. The Clarion–Clipperton Zone (CCZ) in the Pacific Ocean contains some of the world's richest polymetallic nodule deposits, where areas dominated by small nodules have an average abundance of 17 kg m^{-2}, while areas dominated by medium-to-large nodules average 23 kg m^{-2} [1,2]. These nodules form over millions of years through precipitation processes and also the incorporation of particulate material derived from oceanic activities [3,4]. Globally, polymetallic nodules are estimated to contain approximately 7.5 billion tonnes of manganese, 340 million tonnes of nickel, 265 million tonnes of copper, and 78 million tonnes of cobalt [5,6]. As high-grade terrestrial mineral deposits become increasingly depleted, polymetallic nodules are being considered a strategic future source of critical metals to meet the growing demand associated with electrification and energy-transition technologies, particularly for electric-vehicle batteries [7–9].

Polymetallic nodules are highly hydrated, poorly crystalline, and consist of fine-grained minerals, primarily vernadite (δ-$MnO_2 \cdot nH_2O$), todorokite ($(Na,Ca,K)(Mg,Mn^{2+})Mn_6^{4+}O_{12} \cdot 3H_2O$),

and goethite (FeO·OH). These layered and tunnel-structured manganese oxides commonly exhibit variable compositions and mixed manganese oxidation states, while their thermodynamic stability is influenced by hydration, counter-cation content, particle size and surface energy [10].Valuable metals such as copper, cobalt and nickel are heterogeneously disseminated within the Mn–Fe oxide matrix [11–14]. Due to their complex mineralogy and fine-grained nature, conventional mineral processing techniques such as froth flotation and magnetic separation are ineffective for producing a marketable concentrate [15]. Therefore, chemical extraction routes are generally preferred. In many reduction-based processes, the initial step involves reducing Mn(IV) to Mn(II), thereby disrupting the Mn–Fe oxide framework and facilitating the subsequent recovery of valuable metals through downstream hydrometallurgical processing [16].

Pyrometallurgical, hydrometallurgical and hybrid flowsheets have been developed for recovering manganese, nickel, cobalt and copper from the deep-sea polymetallic nodules [17]. Hydrometallurgical approaches, including sulfuric acid leaching, hydrochloric acid leaching and the Cuprion process, have demonstrated high extraction efficiencies for the valuable metals. However, these processes generate large volumes of leach residue and require substantial reagent consumption and waste management, increasing both the operating costs and the environmental impacts [18–21]. Hybrid pyro-hydrometallurgical flowsheets have therefore been developed to address these limitations. Among these, the rotary kiln–electric furnace (RKEF) process is one of the most widely proposed process routes for polymetallic nodules, combining thermal pretreatment and smelting with downstream hydrometallurgical refining to recover copper, nickel and cobalt [22]. Prior to smelting, the polymetallic nodules are typically calcined to remove moisture and phase transformations occur that lower the energy demand of subsequent pyrometallurgical processes. During calcination, the hydrated manganese oxide minerals are converted to lower-valence manganese oxides, disrupting the Mn–Fe oxide framework and preparing the nodules for subsequent carbothermic reduction [11,16,23]. Carbon has been widely investigated as a reductant for selective carbothermic reduction, while carbon monoxide, hydrogen and methane have also been examined as alternative reducing agents [16,23,24]. Rather than achieving complete reduction and smelting, selective carbothermic reduction aims to control the reduction sequence so that valuable metals are preferentially recovered while the manganese remains predominantly in the oxide phase.

Selective carbothermic reduction has been investigated as a pretreatment prior to high-pressure acid leaching [16]. Under the optimum conditions of approximately 600 °C, 3 wt.% carbon and 60 min, Mn(IV) was selectively reduced to Mn(II), disrupting the Mn–Fe oxide lattice and significantly improving the subsequent leaching of copper, nickel and cobalt. Excessive temperatures or carbon additions promoted the metallization of Ni and Co, reducing the effectiveness of the subsequent leaching stage. Maintaining an appropriate reduction window is essential to maximize subsequent leaching while preventing the premature metallization of Ni and Co. More recently, a single-step hydrogen reduction process was developed for recovering Ni, Co and Cu from the polymetallic nodules, for which the authors reported approximately 90% lower CO_2 emissions and about 18% higher metal recovery than the conventional RKEF process [25].

Alternative thermal–hydrometallurgical routes have also been investigated for selective metal recovery from deep-sea polymetallic nodules. Song et al. developed a microwave-assisted ammonium sulfate roasting–leaching process that achieved high extraction efficiencies for Mn (>94%), Cu (>95%), Co and Ni (>75%), while maintaining low iron dissolution (<5%). Although this approach also relies on controlled thermal modification of the nodules, it recovers manganese together with Cu, Ni and Co through leaching rather than selectively producing a Cu–Ni–Co–Fe alloy while retaining manganese in the oxide phase.

Thermodynamic modelling provides an effective means of evaluating complex pyrometallurgical systems before undertaking experimental investigations. Equilibrium calculations using HSC Chemistry and FactSage have been applied to multicomponent metallurgical systems and to the reduction of complex oxide ores [26–30]. Previous thermodynamic modelling of the Mn–O and Mn–O–H systems using HSC Chemistry® demonstrated that manganese-oxide phase stability and decomposition behaviour are strongly influenced by temperature, oxygen partial pressure and atmospheric composition [29]. For polymetallic nodules, thermodynamic studies have demonstrated that the reduction behaviour of manganese, copper, nickel, cobalt and iron can be controlled by appropriate selection of the operating conditions [23,27,31]. Although previous studies have demonstrated the feasibility of selective carbothermic reduction and thermodynamic modelling of polymetallic nodules, they have primarily focused on individual operating conditions or specific process objectives. Consequently, the combined effects of the principal operating variables—including temperature, carbon addition, total pressure, gas atmosphere and nodule composition—on equilibrium phase assemblages, metal recoveries and alloy composition have not been systematically evaluated within a single thermodynamic framework. As a result, the equilibrium operating window for selectively recovering Cu, Ni and Co while limiting iron reduction and suppressing manganese reduction remains insufficiently defined.

To address these knowledge gaps, a representative polymetallic nodule composition was used to develop a thermodynamic model of the selective carbothermic reduction process using HSC Chemistry® 7.1. This paper presents Part I of a two-part investigation on the thermodynamic analysis of a two-stage selective carbothermic process for deep-sea polymetallic nodules, with the objective of establishing the equilibrium operating window for selectively recovering the critical metals Cu, Ni, Co as a Cu–Ni–Co–Fe alloy while suppressing manganese reduction. The equilibrium phase assemblages, metal recoveries and alloy grades were determined as functions of temperature, carbon addition, total pressure, atmosphere composition and nodule composition. Part II presents the thermodynamic design of the subsequent high-temperature reduction stage for producing a ferromanganese–silicide alloy from the manganese-rich residue generated during the first-stage selective carbothermic reduction. The predicted reduction behaviour was also compared with experimental observations reported in previous studies to assess whether the calculated reduction sequence, metal selectivity and effects of temperature and reductant addition are consistent with experimentally observed trends.

2 Thermodynamic Considerations

In order to understand the carbothermic reduction process for polymetallic nodules it is of interest to consider the stabilities of the relevant condensed (solid or liquid) oxides as defined by the standard free energies of the following reactions:

$$2X_{(s\text{ or }l)} + O_{2(g)} = 2XO_{(s\text{ or }l)} \quad (1)$$

and $$4/3Y_{(s\text{ or }l)} + O_{2(g)} = 2/3Y_2O_{3(s\text{ or }l)} \quad (2)$$

and $$Z_{(s\text{ or }l)} + O_{2(g)} = ZO_{2(s\text{ or }l)} \quad (3)$$

where X is a divalent metal cation ($Cu^{2+,}$ Ni^{2+}, Co^{2+}, Fe^{2+}, Mn^{2+}, Mg^{2+}, Ca^{2+}), Y is a trivalent metal cation (Al^{3+}, Mn^{3+}, or Fe^{3+}) and Z is tetravalent silicon (Si^{4+}). The standard free energy change ($\Delta G°$) is defined per mole of oxygen gas. Figure 1 shows the standard free energy changes of the critical battery metal oxides (Cu, Ni and Co), together with manganese, iron, and the major gangue-forming elements Mg, Ca, Al and Si. Copper oxide is the least stable metal oxide and is followed by the nickel and cobalt oxides, which exhibit very similar standard free energies because of their comparable thermodynamic properties. Manganese oxide is a relatively stable oxide, while silica, alumina, calcium oxide and magnesium oxide form very stable oxides. On the other hand, iron oxide has intermediate stability. The large differences in oxide stability suggest that selective reduction of copper, nickel and cobalt should be thermodynamically feasible before significant manganese reduction occurs, thereby providing the fundamental basis for the proposed two-stage selective carbothermic process. For carbothermic reduction, the reduction of the divalent value metal oxide can be described as follows:

$$XO_{(s\text{ or }l)} + C_{(s)} = X_{(s\text{ or }l)} + CO_{(g)} \quad (4)$$

and for the case of silica and silicon:

$$ZO_{2(s\text{ or }l)} + 2C_{(s)} = Z_{(s\text{ or }l)} + 2CO_{(g)} \quad (5)$$

where X is the divalent metal cation ($Cu^{2+,}$ Ni^{2+}, $Co^{2+,}$ Fe^{2+}, Mn^{2+}) and Z is tetravalent silicon (Si^{4+}). The free energy changes (ΔG) per mole of element for these reactions are shown in Figure 2. Copper oxide is a very unstable metal oxide and the free energy change is negative across the whole temperature range. This is followed by nickel oxide, cobalt oxide, and iron oxide. As noted previously, manganese oxide is a very stable oxide and has positive free energy values up to the high end of the temperature range. Silica exhibits the highest free energy values and therefore is the most thermodynamically stable oxide considered.

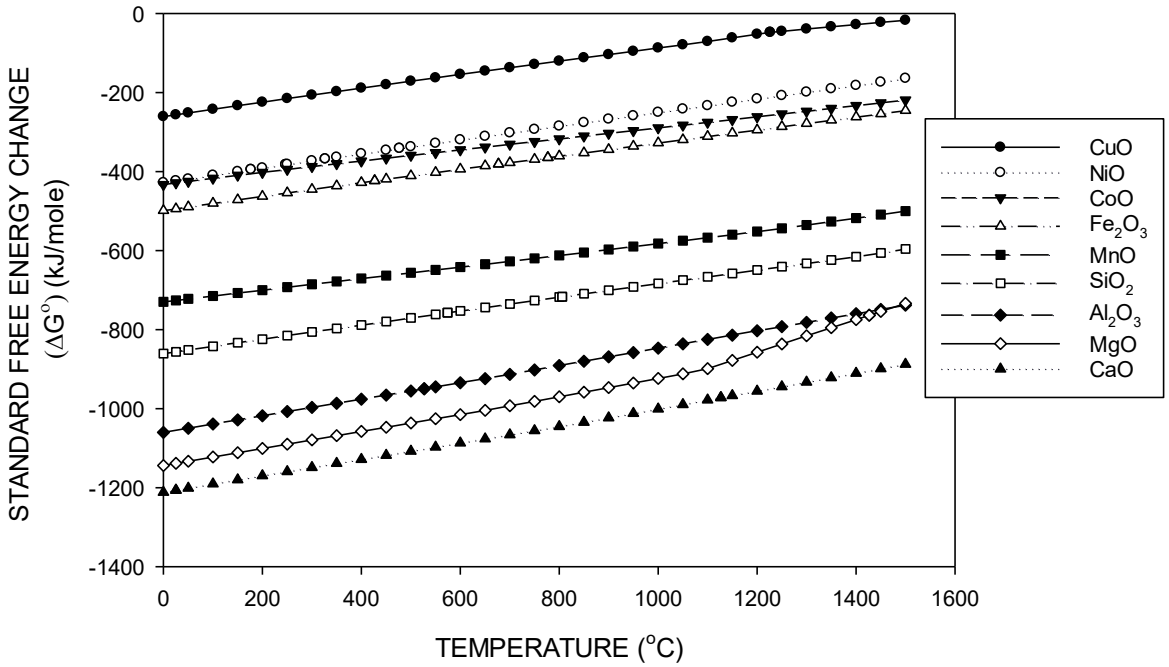


Figure 1 Standard free energy changes (ΔG^o) per mole of oxygen gas as a function of temperature for the oxides of interest.

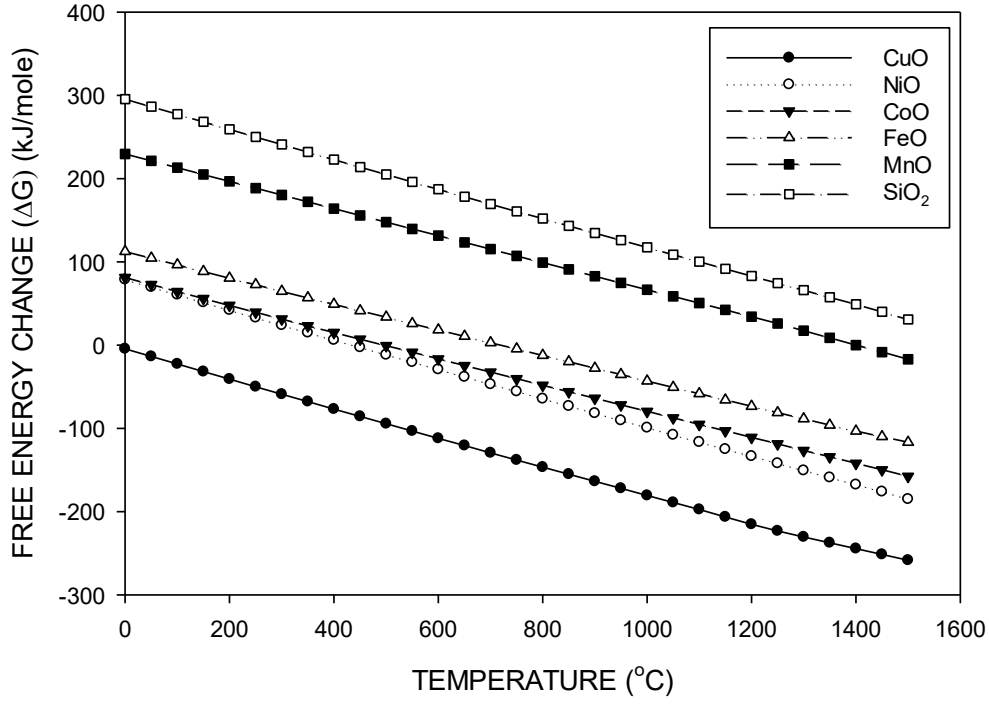


Figure 2 Free energy changes (ΔG) as a function of temperature for the carbothermic reduction of the oxides of interest.

3 Thermodynamic Model Development

In order to investigate the carbothermic reduction of deep-sea polymetallic nodules, a thermodynamic model was developed using HSC Chemistry® 7.1 [32]. The Equilibrium Composition module was used to study the multicomponent equilibrium of the heterogeneous system, consisting of the nodules plus a reducing agent. The Gibbs solver, which utilizes the Gibbs free energy minimization technique, was employed to determine the equilibrium composition of the reacted system under isobaric and isothermal conditions. The input consisted of the chemical composition of the polymetallic nodules as well as the amounts of any additions, such as carbon, used as a reducing agent. All the species that were initially present in the nodules, as well as those that could potentially form during the process, were specified. The module automatically generates these species, and they are grouped into various phases, typically gas, oxide and metal phases. The process atmosphere was also specified in the model because it influences the equilibrium gas composition. For this purpose, nitrogen was included as a gaseous species and thus it was necessary to define the atmospheric conditions under which the process operates. The atmosphere could be, for example, the gases produced during the reduction process, nitrogen, an inert gas such as argon or operation under reduced atmospheric pressure. The variables investigated were the temperature, the amount of carbon, the atmospheric conditions and the nodule composition.

It should be noted that the model has a number of limitations. Firstly, the model assumes that the system is closed and thus any gases that are produced remain in the system. In an actual reactor, the gases could potentially escape, thereby reducing the partial pressures of the product gases. Secondly, the thermodynamic data in the HSC Main database (MainDB) are assumed to be accurate. If thermodynamic data are not available in the MainDB database, they can be added via the Own database (OwnDB). Furthermore, for a given species, the data in the OwnDB database supersede that in the MainDB database. Thirdly, it is assumed that the high-temperature reactions occur rapidly, equilibrium is achieved and thus kinetics are not considered. Finally, ideal (Raoultian) behaviour is assumed for all species within each phase. However, if the behaviour is non-ideal and activity-coefficient data are available, these data can be incorporated into the model.

The chemical composition of the nodules used in the present study is given in Table 1, with the elements represented in oxide form. The concentrations of the critical battery metal oxides were 1.18 wt.% CuO, 1.36 wt.% NiO and 0.15 wt.% CoO, while the manganese oxide concentration was 32.0 wt.% MnO. The Fe_2O_3 concentration was 8.85 wt.%. The Loss-on-Ignition (LOI) was 26.8 wt.%, indicating the presence of a substantial amount of structurally bound and free water. The total sum of the oxides plus LOI was 96.2 wt.%, and the remaining 3.8 wt.% was likely due to the presence of other species and additional oxygen associated with higher oxidation-state manganese species. For example, manganese occurs predominantly as Mn(IV) within minerals such as vernadite and todorokite rather than solely as MnO.

Table 1 Chemical composition of polymetallic nodules in oxide form

SiO_2 %	**Al_2O_3** %	**Fe_2O_3** %	**MgO** %	**CaO** %	**Na_2O** %	**K_2O** %	**TiO_2** %	**P_2O_5** %
13.9	3.62	8.85	2.63	2.00	1.89	0.92	0.38	0.31
MnO %	**Cr_2O_3** %	**V_2O_5** %	**CuO** %	**CoO** %	**NiO** %	**ZnO** %	**LOI** %	**Total** %
32.0	< 0.01	0.08	1.18	0.15	1.36	0.17	26.8	96.2

For the purpose of the calculations, the oxide concentrations were normalized to one hundred percent and the species considered in the calculations are shown in Table 2. Elements present in small amounts (<1 wt.%), such as titanium, chromium, vanadium, phosphorus and zinc oxides, were not included. Cobalt was retained, since it is of significant economic value despite its relatively low concentration and is usually recovered with nickel and copper. Inputting the elements in Table 2, together with oxygen and carbon, into the Equilibrium Composition module generated a list of 377 possible equilibrium species. However, many of these were unstable under the conditions investigated and consequently their equilibrium concentrations were negligible or zero. Therefore, to facilitate the calculations, these species were not included in the subsequent equilibrium modelling. The species considered in the calculations are shown in Table 3 and they were grouped into five phases: gases, condensed oxides, Alloy I, Alloy II and carbon.

The carbon addition was expressed as kilomoles of carbon per 100 kilograms (kmole C /100 kg) of nodules. For the purpose of the calculations all the water (LOI) was assumed to be removed. This assumption is supported by our previous experimental studies, which demonstrated that polymetallic nodules can be extensively dewatered using microwave heating. Maximum mass losses of 31% at the bench scale and 24.8% at the pilot scale were achieved, confirming the practical feasibility of moisture removal prior to carbothermic reduction [33,34]. To account for the solubility of species such as carbon and silicon in Alloy II, it was assumed to consist of Fe, Mn, Si and C. The alloy composition was calculated by summing the equilibrium amounts of all elemental, carbide and silicide species present in the alloy phase. Thus, iron was determined from the amounts of Fe, Fe_3C and FeSi; manganese from Mn, Mn_7C_3 and Mn_3Si; silicon from Si, FeSi, Mn_3Si and SiC; and carbon from Fe_3C, Mn_7C_3 and SiC.

Table 2 Normalized chemical composition of polymetallic nodules as used in the model

SiO_2 %	**Al_2O_3** %	**Fe_2O_3** %	**MgO** %	**CaO** %	**Na_2O** %
14.73	3.84	9.38	2.79	2.12	2.00
MnO %	**CuO** %	**CoO** %	**NiO** %	**LOI** %	**TOTAL** %
33.91	1.25	0.16	1.44	28.38	100.00

Table 3 Phases (in bold) and species (unbold) that were used in the thermodynamic model

GASES	**OXIDES**	**OXIDES**	**OXIDES**	**OXIDES**	**OXIDES**	**ALLOY I**
$CO_{(g)}$	Al_2O_3	$2CaO{\cdot}SiO_2$	$CuO{\cdot}Al_2O_3$	Mg_2SiO_4	Na_2O	Cu, Ni, Co
$CO_{2(g)}$	$Al_2O_3{\cdot}SiO_2$	$(Ca,Fe)_{0.5}SiO_3$	FeO	Mn_2O_3	$NaMnO_4$	Fe
$O_{2(g)}$	$MgO{\cdot}Al_2O_3$	$(Mn,Ca)SiO_3$	Fe_3O_4	MnO_2	Na_2SiO_3	**ALLOY II**
$SiO_{(g)}$	CaO	CoO	Fe_2O_3	MnO	$NaAlSiO_4$	Mn, Si
$N_{2(g)}$	$CaSiO_3$	$CoFe_2O_4$	$FeSiO_3$	Mn_3O_4	$Na_2O{\cdot}2SiO_2$	Fe
$Mn_{(g)}$	$CaMgSi_2O_6$	$CoMn_2O_4$	$2FeO{\cdot}SiO_2$	$MnO{\cdot}Fe_2O_3$	NiO	Fe_3C, Mn_7C_3, SiC
$Mg_{(g)}$	$(Ca,Mg)_{0.5}SiO_3$	CuO	MgO	Mn_2SiO_4	$NiFe_2O_4$	FeSi, Mn_3Si
$Na_{(g)}$	$(Ca,Mg)SiO_4$	$CuFe_2O_4$	$MgFe_2O_4$	$CuFeO_2$	$NiMn_2O_4$	**CARBON**
$Cl_{2(g)}$	$Ca_3Si_2O_7$	$CuMn_2O_4$	$MgSiO_3$	$MnSiO_3$	SiO_2	C

Some activity coefficients and thermodynamic data from the literature were added to the model. The activity coefficient data for copper and nickel were obtained from the activity data of Rapp and Maak at 700 °C and 1000 °C [35]. Both copper and nickel exhibit positive deviations from ideality. Their data were fitted to the following expressions:

$$\ln \gamma_{Cu} = (2.79 - 1.13x10^{-3}T) + (-8.33 + 4.00x10^{-3}T)X_{Cu} + (8.54 - 4.93x10^{-3}T)X_{Cu}^2 + (-3.00 + 2.05x10^{-3}T)X_{Cu}^3 \quad (6)$$

$$\ln \gamma_{Ni} = (1.90 - 6.49x10^{-4}T) + (-4.03 + 1.69x10^{-3}T)X_{Ni} + (3.77 - 2.36x10^{-3}T)X_{Ni}^2 + (-1.71 + 1.37x10^{-3}T)X_{Ni}^3 \quad (7)$$

Cobalt was assumed to have the same activity coefficient as nickel. In order to model the behaviour of the various compounds formed between copper, nickel or cobalt and manganese oxide, it was necessary to input additional thermodynamic data into the OwnDB for the following species: $CuMn_2O_4$, $NiMn_2O_4$ and $CoMn_2O_4$. For $CuMn_2O_4$ and $NiMn_2O_4$, the standard enthalpy and entropy values were available in the MainDB; however, heat-capacity data were not available. Therefore, the heat-capacity values were estimated using the Neumann–Kopp rule, which assumes that the heat capacity of a mixed oxide is equal to the weighted sum of the heat capacities of its constituent oxides. The standard enthalpy and entropy values, together with the estimated heat-capacity coefficients, are shown in Table 4. For $CoMn_2O_4$, neither the standard enthalpy nor the standard entropy of formation was available. Therefore, the standard enthalpies and entropies of formation for XMn_2O_4 (X = Cu or Ni) and YFe_2O_4 (Y = Cu, Ni or Co) were compared with the values calculated using the Neumann–Kopp rule. Good agreement was obtained for the copper- and nickel-containing compounds, indicating that the estimation method was sufficiently accurate. Consequently, the calculated thermodynamic properties for $CoMn_2O_4$, as listed in Table 4, were added to the HSC OwnDB.

Table 4 Entropy, enthalpy and heat capacity values for $CuMn_2O_4$, $NiMn_2O_4$ and $CoMn_2O_4$.

SPECIES	ΔH^0 kJ/mol	ΔS^0 J/(mol·K)	A J/(mol·K)	B J/(mol·K)	C J/(mol·K)	D J/(mol·K)
$CuMn_2O_4$	-1109.2	146.4	152.1	42.3	-21.0	0.001
$NiMn_2O_4$	-1122.2	142.3	214.0	-220.6	-35.7	353.2
$CoMn_2O_4$	-1196.9	163.4	154.8	35.3	-10.7	4.3

4 Results and Discussion

4.1 Preliminary Thermodynamic Basis for the Selective Reduction Process

It is of interest to perform a preliminary investigation of the overall reduction of the nodules to determine the ranges of the key operating parameters governing the selective reduction process,

particularly the carbon requirements and operating temperatures. Based on the oxide stability information discussed previously, in Stage I, the copper, nickel and cobalt oxides are relatively unstable and are reduced to produce Alloy I according to the following carbon-consuming reactions:

$$CuO_{(s\ or\ l)} + C_{(s)} = Cu_{(s\ or\ l)} + CO_{(g)} \quad (8)$$

$$NiO_{(s\ or\ l)} + C_{(s)} = Ni_{(s\ or\ l)} + CO_{(g)} \quad (9)$$

$$CoO_{(s\ or\ l)} + C_{(s)} = Co_{(s\ or\ l)} + CO_{(g)} \quad (10)$$

In addition to the reduction of the unstable metal oxides, MnO_2 and Fe_2O_3 are expected to undergo stepwise reduction to their lower-valence oxides and in the case of iron oxide to metallic iron, thereby consuming carbon without producing metallic manganese, according to the following reaction sequences:

For manganese: $$2MnO_{2(\ s\ or\ l)} + C_{(s)} = Mn_2O_{3_{(s\ or\ l)}} + CO_{(g)} \quad (11)$$

$$3Mn_2O_{3_{(s\ or\ l)}} + C_{(s)} = 2Mn_3O_{4_{(s\ or\ l)}} + CO_{(g)} \quad (12)$$

$$Mn_3O_{4_{(s\ or\ l)}} + C_{(s)} = 3MnO_{(s\ or\ l)} + CO_{(g)} \quad (13)$$

For iron: $$3Fe_2O_{3_{(s\ or\ l)}} + C_{(s)} = 2Fe_3O_{4_{(s\ or\ l)}} + CO_{(g)} \quad (14)$$

$$Fe_3O_{4_{(s\ or\ l)}} + C_{(s)} = 3FeO_{(s\ or\ l)} + CO_{(g)} \quad (15)$$

$$FeO_{(s\ or\ l)} + C_{(s)} = Fe_{(s\ or\ l)} + CO_{(g)} \quad (16)$$

The sequence is consistent with the established thermodynamic stability order of the principal manganese oxides: MnO_2, Mn_2O_3, Mn_3O_4 and MnO with progressively decreasing oxygen potential [29]. According to the above equations, the stoichiometric amount of carbon required to reduce the copper, nickel and cobalt oxides is 0.037 kmole C/100 kg of nodules. However Fe_2O_3 will be reduced to at least FeO, and manganese dioxide will be reduced to MnO. The additional carbon required to reduce the higher-valence iron and manganese oxides to FeO and MnO is 0.537 kmole C/100 kg of nodules, giving a total carbon addition of 0.574 kmole C/100 kg of nodules.

Figure 3 shows the equilibrium distribution of the principal metallic components as a function of temperature for this carbon addition. The maximum amount of nickel occurs at approximately 700 °C, where the recoveries of copper and cobalt are also high. At this temperature, Alloy I consists predominantly of Cu, Ni and Co with only a limited amount of dissolved iron, indicating highly selective recovery of the metals. Although some iron is reduced into Alloy I, its amount increases rapidly above 700 °C, indicating a progressive loss of selectivity at higher temperatures. The iron content of Alloy I reaches a maximum at approximately 850 to 900 °C before decreasing as iron progressively partitions into Alloy II at higher temperatures. In contrast, manganese remains largely unreduced within this temperature range and only begins to transfer to Alloy II at approximately 1350 to 1400 °C, followed by a rapid increase in manganese recovery with

increasing temperature. Silicon reduction occurs over a similar temperature range but to a much smaller extent, reflecting the significantly greater thermodynamic stability of silica as compared to manganese oxide. The transfer of iron from Alloy I to Alloy II at elevated temperatures coincides with the onset of manganese reduction, indicating the progressive formation of a ferromanganese–silicon alloy. Above approximately 1500 °C, the amounts of iron and manganese in Alloy II approach relatively constant values, suggesting that equilibrium has largely been established for the selected carbon addition.

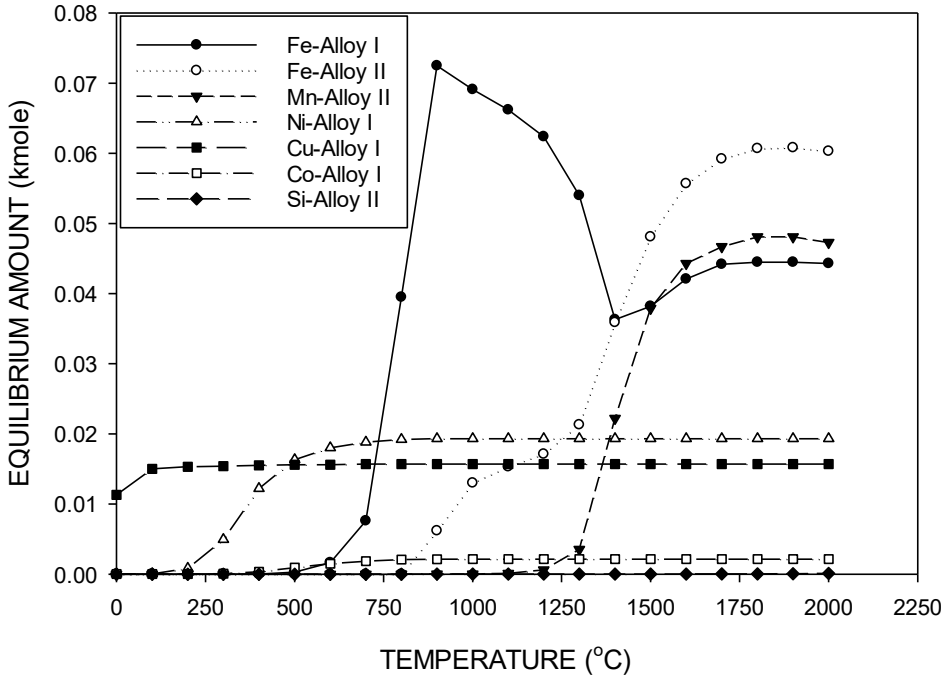


Figure 3 Thermodynamic basis for the proposed two-stage selective carbothermic reduction of deep-sea polymetallic nodules.

4.2 Stage I - Selective Reduction of Copper, Nickel and Cobalt - Alloy I

Based on the above discussion, of particular importance for the selective reduction of the copper, nickel and cobalt oxides to produce a Cu–Ni–Co alloy (Alloy I) are the carbon requirement and the temperature. Here it would be expected that the MnO_2 and the Fe_2O_3 would be reduced by carbon to their lower oxidation-state oxides, thereby consuming carbon without producing metallic manganese, according to reactions (11)-(16). Figures 4(a) and (b) show the equilibrium amounts of the manganese-containing and iron-containing species, respectively, as a function of carbon addition at 700 °C, which corresponds approximately to the optimum temperature for selective recovery of the metals.

The behaviour of the manganese-containing species can be divided into three regions: low carbon additions, medium carbon additions and high carbon additions. At low carbon additions MnO_2 and Mn_2O_3 are present in progressively decreasing amounts as the carbon addition

increases. Correspondingly, the amount of Mn_3O_4 increases. Increasing carbon addition promotes the sequential reduction of the manganese oxides from MnO_2 to Mn_2O_3, then to Mn_3O_4, before MnO becomes the dominant manganese-bearing phase [36]. This predicted progression towards lower-valence manganese oxides is qualitatively consistent with our previous TGA/DTGA observations for polymetallic nodules, which showed mass-loss regions between 300 and 700 °C attributed to the collapse of the todorokite tunnel structure and a further region between 850 and 950 °C that may be associated with the thermal reduction of MnO_2 to MnO [34]. Also, the amounts of the manganese silicates ($(Mn,Ca)SiO_3$ and $MnSiO_3$) and manganese ferrite ($MnFe_2O_4$) increased and reached their maxima in the medium carbon addition range. Subsequently, their amounts decreased and the amount of MnO began to increase rapidly, particularly above approximately 0.15 kmole C/100 kg, with the amount levelling off at a carbon addition of about 0.20 to 0.22 kmole C/100 kg. Here MnO predominates; however, some of the manganese silicates remain present at high carbon additions indicating that complete conversion of manganese into MnO is not thermodynamically favoured under these conditions. Similarly, some $MnFe_2O_4$ also remains. NaMnO4 exists across the whole carbon addition range, indicating that it is a stable species. The above results for the manganese-containing species demonstrate that, in addition to the carbon required for the reduction of the metal oxides, supplementary carbon must be added to reduce the higher oxidation-state manganese oxides to MnO.

In a manner similar to the manganese species, the behaviour of the iron-containing species can be divided into the same three carbon addition ranges. At low carbon additions, the primary species is Fe_2O_3, together with some $NiFe_2O_4$. With increasing carbon, the Fe_2O_3 is progressively replaced by Fe_3O_4, and the $NiFe_2O_4$ is replaced by $MnFe_2O_4$. Finally, the amounts of Fe_3O_4 and $MnFe_2O_4$ decrease and the predominant species becomes FeO. The amount of FeO begins to level off at a carbon addition of about 0.26 to 0.28 kmole C/100 kg, indicating that most of the iron is present as FeO under these conditions. Thus, as noted for the manganese-containing species, supplementary carbon is required to reduce the iron oxides to at least FeO to achieve the selective reduction of copper, nickel and cobalt.

Furthermore, metallic iron begins to form at a carbon addition of approximately 0.17 kmole C/100 kg, coinciding with the onset of FeO reduction. Thereafter, the amount of metallic iron increases gradually with increasing carbon addition. The progressive reduction of iron oxide with increasing carbon addition is consistent with previous thermodynamic studies, which also reported increasing iron incorporation into the alloy under more strongly reducing conditions [36]. As noted above, the carbon requirement for the highest recoveries of copper, nickel and cobalt is in the range of 0.28 to 0.35 kmole C/100 kg. This range can be contrasted with the theoretical carbon addition requirement of only 0.037 kmole C/100 kg for the reduction of only the copper, nickel and cobalt oxides. The large difference between the theoretical and optimum carbon additions confirms that most of the carbon consumed during Stage I is associated with reducing the higher oxidation-state manganese and iron oxides rather than the metal oxides themselves. Additionally, the copper–nickel–cobalt alloy will contain some iron since metallic iron forms well before the optimum carbon addition range is reached. Consequently, complete suppression of iron reduction is

thermodynamically impossible under the conditions required for the high recoveries of copper, nickel and cobalt, although the amount of iron incorporated into Alloy I remains relatively limited.

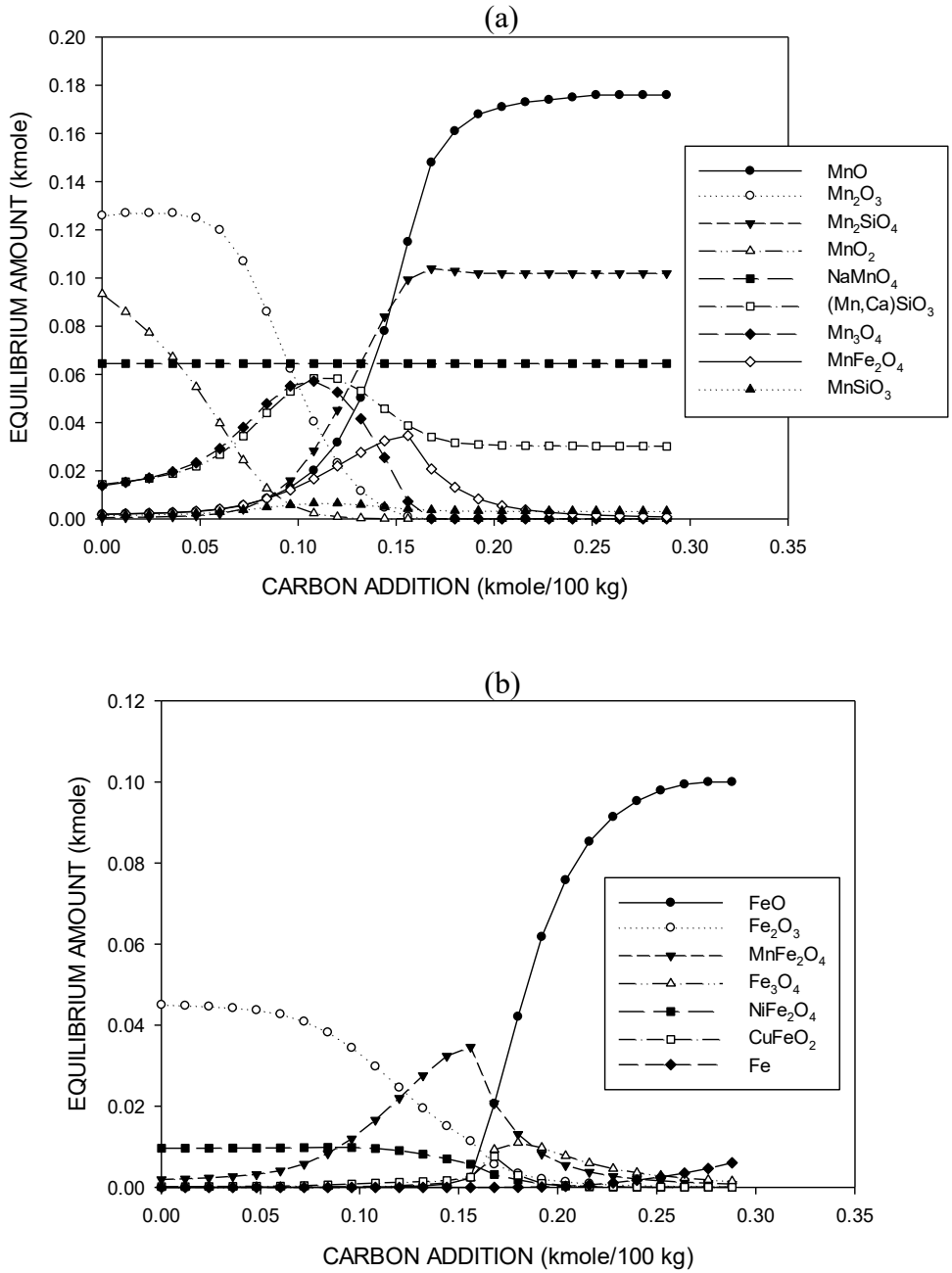


Figure 4 Equilibrium amounts of (a) manganese-containing and (b) iron-containing species as a function of carbon addition at 700 °C.

The behaviour of the nickel-bearing, copper-bearing and cobalt-bearing species is shown as a function of carbon addition at 700 °C in Figures 5(a), (b) and (c), respectively. At low carbon additions, CuO and $CuAl_2O_4$ are the predominant species, but as the carbon addition increases $CuAl_2O_4$ is replaced by $CuFeO_2$. This intermediate phase reaches a maximum at a carbon addition

of approximately 0.17 kmole C/100 kg before decreasing rapidly as metallic copper forms. At even higher carbon additions, copper metal begins to form in increasing amounts and becomes the predominant species. The amount of copper begins to level off at about 0.23 kmole C/100 kg, indicating essentially complete reduction of the copper-bearing phases. For nickel, at low carbon additions, NiO, $NiFe_2O_4$ and $NiMn_2O_4$ are present in substantial amounts. With increasing carbon addition, the amounts of $NiFe_2O_4$ and $NiMn_2O_4$ decrease and the amount of NiO initially increases as these mixed oxides decompose. Subsequently, this NiO is reduced to nickel metal, which becomes the predominant species, with the amount levelling off at a carbon addition of about 0.28 kmole C/100 kg. The temporary increase in NiO demonstrates that the mixed nickel oxides are thermodynamically less stable than NiO and are therefore reduced through an intermediate oxide stage before metallic nickel is produced. Cobalt behaves in a manner very similar to nickel, with CoO, $CoFe_2O_4$ and $CoMn_2O_4$ being present at low carbon additions, followed by the progressive decomposition of the mixed oxides to CoO and the subsequent reduction of CoO to metallic cobalt. Cobalt metal becomes the predominant species at high carbon additions, although a small amount of $CoFe_2O_4$ persists throughout the investigated carbon addition range. The cobalt recovery begins to level off at a slightly higher carbon addition of approximately 0.30 kmole C/100 kg. This slightly higher carbon requirement for cobalt as compared with copper and nickel is consistent with the slightly greater thermodynamic stability of CoO, as discussed previously.

A comparison of Figures 5(a)–(c) shows that copper is reduced at the lowest carbon additions, followed by nickel and then cobalt. This sequence is in excellent agreement with the thermodynamic stability of the corresponding oxides presented in Figures 1 and Figure 2. Although the reduction pathways differ because of the formation and decomposition of intermediate mixed oxides, within the carbon addition range of approximately 0.28 to 0.30 kmol C/100 kg at 700 °C, copper and nickel are nearly completely reduced, whereas the cobalt recovery reaches approximately 86.5%. Increasing the carbon addition to 0.35 to 0.40 kmol C/100 kg improves the cobalt recovery to approximately 97%, but also increases the iron reduction and decreases the selectivity. The carbon requirement closely corresponds to the operating window identified for Stage I and confirms that selective recovery of the metals can be achieved before significant manganese metallization occurs. The predicted increase in iron reduction with increasing carbon addition is consistent with the previous thermodynamic studies [36].

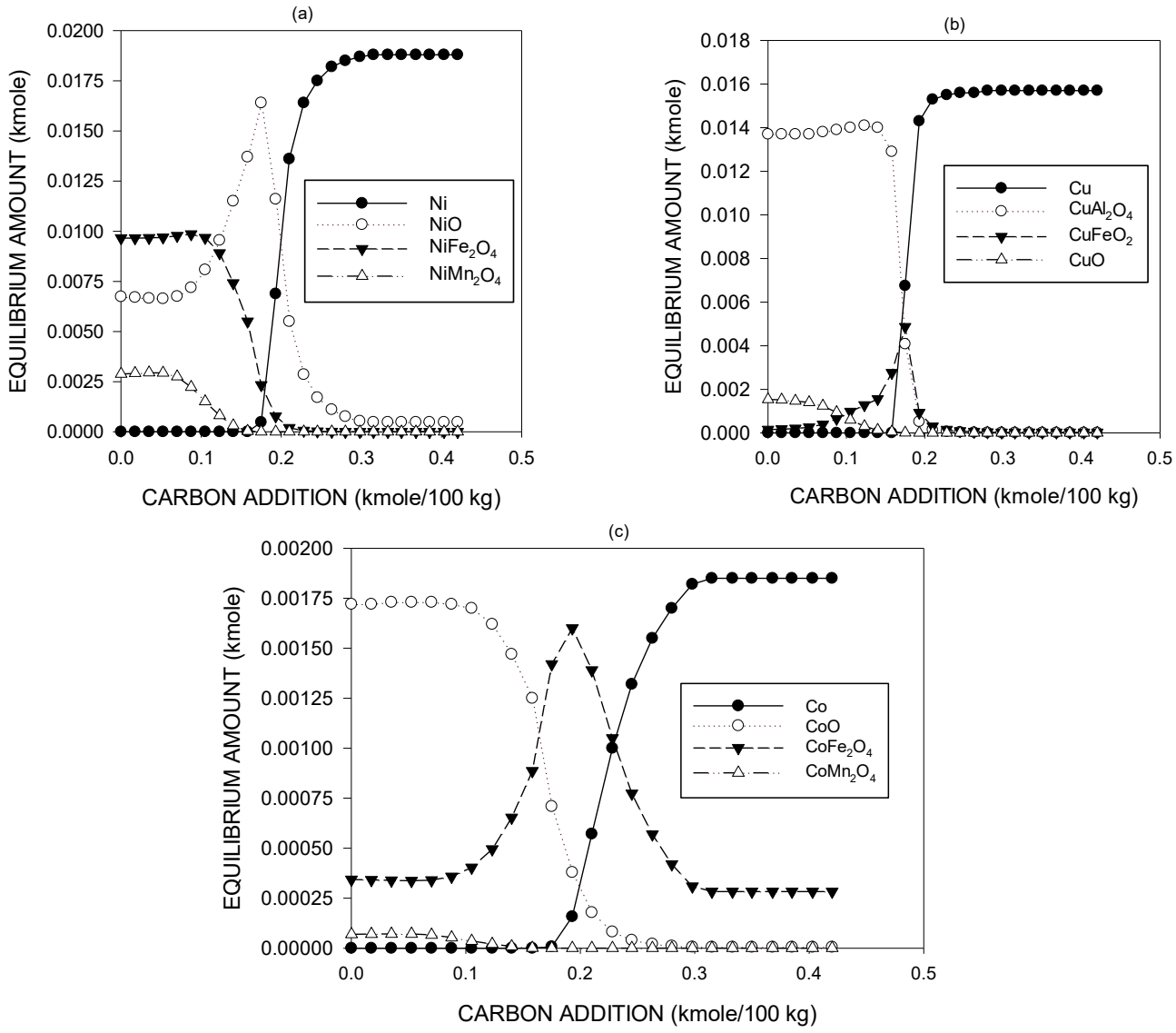


Figure 5 Equilibrium amounts of (a) copper, (b) nickel and (c) cobalt as a function of carbon addition at 700 °C.

The recoveries and grades of the metals in Alloy I are shown as a function of carbon addition at 700 °C in Figures 6(a) and (b), respectively. Copper is the first metal to be recovered, with its recovery increasing rapidly over a narrow carbon-addition range. This is followed by rapid increases in the recoveries of nickel and then cobalt and finally iron. The recovery of iron increases more gradually than those of the other metals. Copper achieved the maximum recovery and this was followed by nickel, cobalt and iron, with maximum recoveries of 99.8%, 97.5%, 86.5% and 6.9%, respectively. The maximum iron recovery occurred at approximately the same carbon addition as the maximum amounts of the other metals indicating that limited iron reduction is unavoidable under the conditions required for maximum metal recovery. There was an insignificant amount of manganese recovered, confirming that manganese remains predominantly in the oxide phase throughout Stage I.

With regard **to** the metal grades, initially the copper content is high as it is recovered first, but its concentration drops rapidly as nickel, cobalt and iron are produced in increasing amounts. At low carbon additions, the alloy therefore consists predominantly of copper, whereas increasing carbon additions progressively enrich the alloy in nickel, cobalt and iron. For the maximum recoveries, the copper, nickel, cobalt and iron grades are 37.4%, 41.4%, 4.1% and 17.1%, respectively. Above approximately 0.30 kmole C/100 kg, the alloy composition remains essentially constant, indicating that equilibrium has been established and further carbon additions have little influence on either the recovery or the alloy grade. A lower iron content could be achieved at lower carbon additions below approximately 0.3 kmole C/100 kg, but this would be at the expense of high recoveries, particularly of nickel and cobalt. Consequently, the optimum carbon addition represents a compromise between maximizing the recoveries of the critical metals and minimizing iron incorporation into Alloy I.

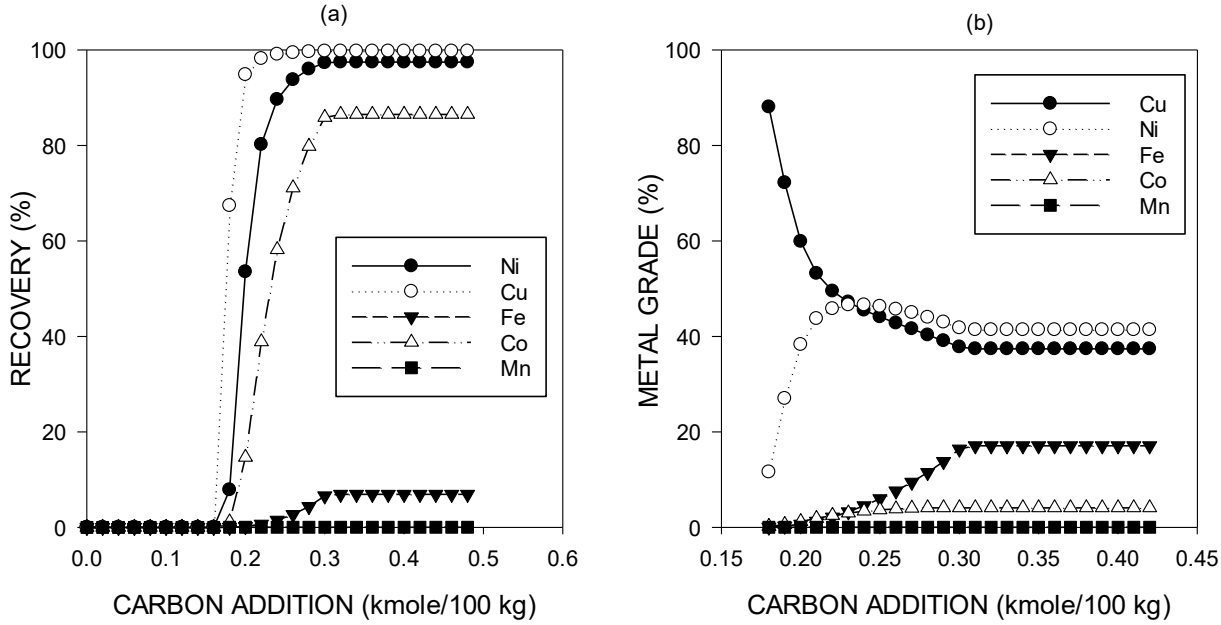


Figure 6 (a) Recoveries and (b) grades of the value metals in Alloy I as a function of carbon addition at 700 °C.

Figures 7(a) to (c) show three-dimensional mesh plots of the metal recoveries for copper, nickel and cobalt in Alloy I as a function of carbon addition and temperature. With regards to copper, as noted previously, copper oxide is an unstable oxide and thus reduction occurs readily at low carbon additions and particularly low temperatures. However, in comparison to the stoichiometric requirement of 0.016 kmole C/100 kg for copper oxide alone, copper is only recovered at carbon additions above about 0.15 kmole C/100 kg as this additional carbon is utilized to reduce the higher oxides of manganese and iron to the lower oxides. Copper metal is stable at room temperature and metal recoveries of approximately 95% can be achieved at a low temperature of approximately 150 °C. Recoveries of approximately 98% are achieved at and above approximately 325 °C and at carbon additions above approximately 0.15 kmole C/100 kg. The relatively broad plateau observed in Figure 7(a) indicates that copper recovery is comparatively insensitive to further increases in

either temperature or carbon addition once these conditions are reached. At high temperatures and low carbon additions the copper recovery begins to drop, and this is attributed to equilibrium reoxidation as the HSC Equilibrium program assumes a closed system.

NiO, being a substantially more stable oxide than copper oxide, requires stronger reducing conditions. Nickel metal does not form until about 200 °C. Therefore, to achieve the same recovery as for copper of approximately 98%, a temperature of about 700 °C and a carbon addition above about 0.30 kmole C/100 kg are required. Once more, the need for a carbon addition beyond the stoichiometric requirement of 0.035 kmole C/100 kg for both the copper and nickel oxides is attributed to the reduction of the higher oxides of both manganese and iron to the lower oxides. Compared with copper, the recovery surface for nickel is shifted towards higher temperatures and carbon additions, reflecting the greater thermodynamic stability of nickel oxide. Yet again, reoxidation occurs at low carbon additions and high temperatures.

Regarding cobalt, the thermodynamic properties of the cobalt and nickel oxides are similar. However, cobalt oxide is present in much smaller concentrations than nickel oxide (0.019 kmole NiO as compared with 0.002 kmole CoO), by almost a factor of ten, and this results in cobalt oxide being more difficult to reduce. Accordingly, the maximum recovery of approximately 97% is only achieved at a high carbon addition of approximately 0.403 kmole C/100 kg and a high temperature of approximately 800 °C. The recovery surface for cobalt is therefore displaced to slightly higher temperatures and carbon additions than that for nickel, indicating that cobalt requires the strongest reducing conditions of the three metals. Again, reoxidation is predicted at low carbon additions and high temperatures because of the closed-system equilibrium assumption employed in the calculations.

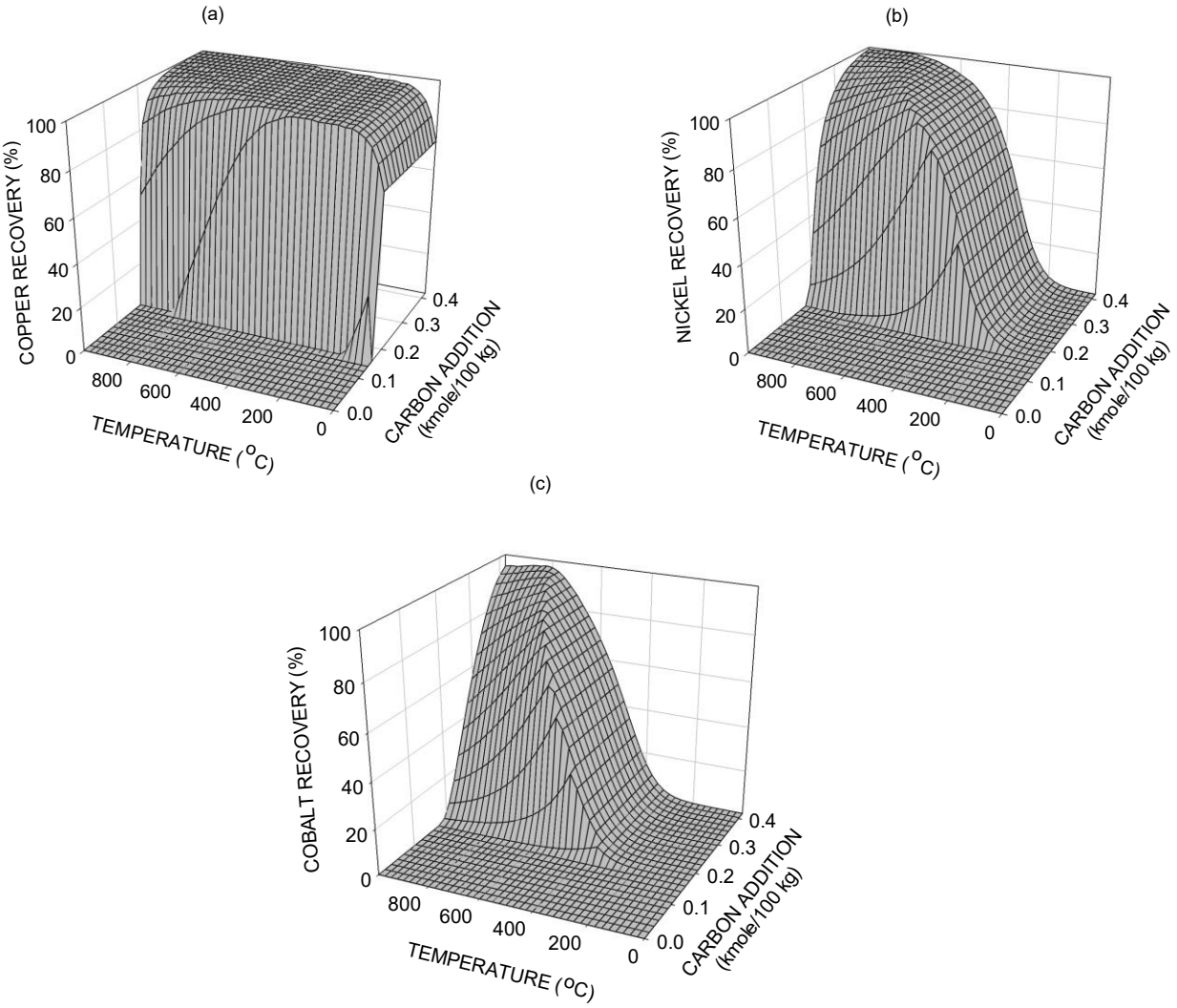


Figure 7 Recoveries of (a) copper, (b) nickel and (c) cobalt in Alloy I as a function of temperature and carbon addition

Figures 8(a) and (b) show the iron recoveries and grades for Alloy I, respectively, as a function of both carbon addition and temperature. At approximately 725 °C the iron recovery is about 10% at a carbon addition of approximately 0.333 kmole C/100 kg. Above about 600 °C, the iron recovery and grade both increase rapidly with increasing temperature and carbon addition. However, the highest iron recoveries and grades are only achieved under substantially stronger reducing conditions than those required for the selective recovery of the critical metals. At approximately 700 °C and a carbon addition of approximately 0.30 kmole C/100 kg, which corresponds to the conditions required for approximately 98% nickel recovery, the iron grade is about 16%. Thus, the low-temperature selective reduction of the nodules results in the production of an alloy containing mainly copper, nickel and cobalt together with a limited amount of iron. The relatively low iron recovery under these conditions confirms that the selective reduction process effectively suppresses excessive iron metallization while maintaining high recoveries of the metals.

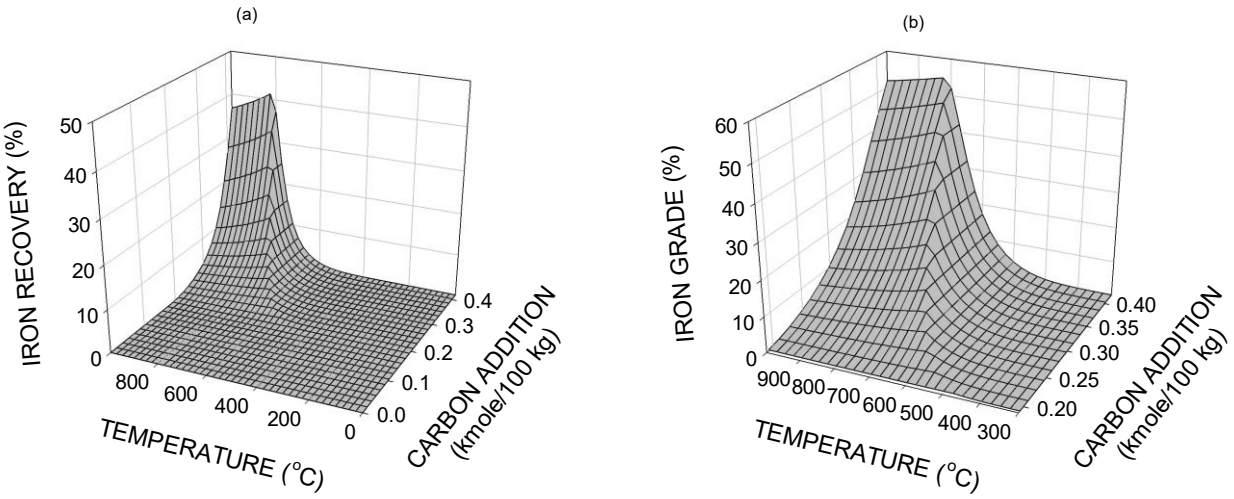


Figure 8 (a) Iron recoveries and (b) iron grade in Alloy I as a function of temperature and carbon additions.

The sensitivity of manganese-oxide equilibria to pressure and atmospheric composition has been demonstrated in previous thermodynamic modelling of the Mn–O and Mn–O–H systems [29]. The effect of atmospheric conditions on the metal recoveries was investigated by either reducing the operating pressure or by adding an essentially inert gas such as nitrogen. In both cases, the recoveries would be expected to increase as the partial pressures of the gaseous products, such as carbon monoxide, are reduced. Figures 9(a), (b), (c) and (d) show the effect of reducing the atmospheric pressure on the recoveries of copper, nickel, cobalt and iron, respectively, as a function of temperature for a carbon addition of 0.250 kmole C/100 kg. In all cases the recovery increases with decreasing pressure, particularly at the lower pressures. This is consistent with Le Chatelier's principle, as reducing the carbon monoxide partial pressure promotes the forward reduction reactions. For copper, since the recovery is high even at low temperatures, the effect of pressure is not significant over the temperature range of about 700 to 725 °C. Similarly, for nickel and cobalt, at the temperatures where high recoveries are achieved, there are only slight improvements in the recoveries at low pressures for the conditions chosen. The greatest influence of pressure occurs at intermediate temperatures, where the reduction reactions are close to equilibrium, whereas once the recovery plateau is reached the effect of pressure becomes negligible. On the other hand, iron shows a much stronger dependence on operating pressure, with the recovery increasing significantly at low pressures. This indicates that iron reduction is more sensitive to changes in carbon monoxide partial pressure than the reduction of the critical metals under the selected conditions. However, since the increased recovery of iron lowers the metal alloy grade, operation at reduced pressure is unlikely to provide a significant practical benefit during Stage I. The relatively small improvements in copper, nickel and cobalt recoveries are outweighed by the increased iron recovery and the associated reduction in alloy selectivity.

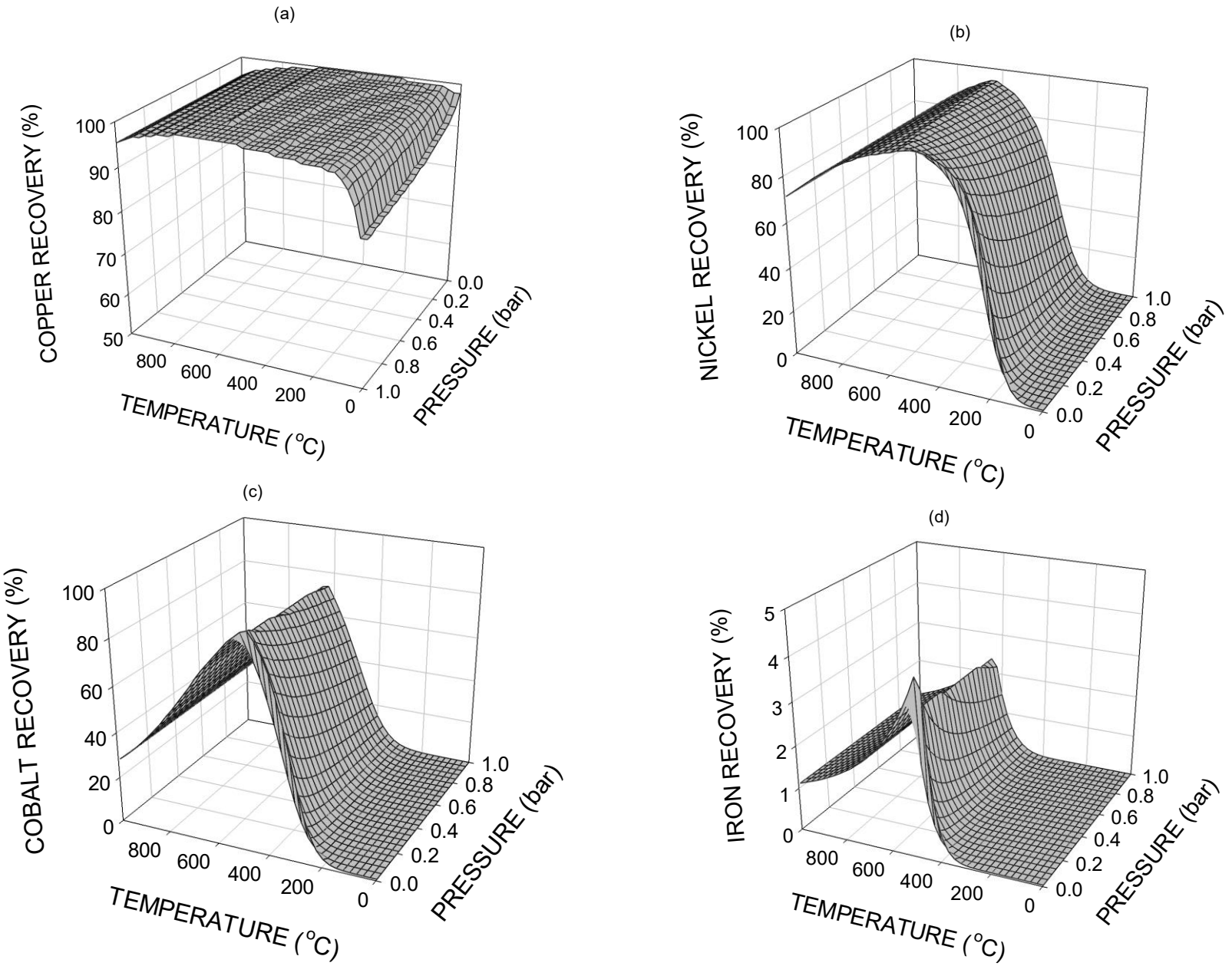


Figure 9 (a) Copper, (b) nickel, (c) cobalt and (d) iron recoveries in Alloy I as a function of temperature and atmospheric pressure for a carbon addition of 0.25 kmole C/100kg

The effect of nitrogen additions on the recovery of the four metals is shown in Figures 10(a), (b), (c) and (d), respectively, again as a function of temperature and for a carbon addition of 0.250 kmole C/100 kg. The results are similar to those for reduced atmospheric pressure, with the metal recoveries increasing with increasing nitrogen additions. This is also consistent with Le Chatelier's principle, as dilution of the gaseous reaction products reduces their partial pressures and thereby promotes the forward reduction reactions. Again, since copper is relatively readily recovered, the effect of nitrogen on the copper recovery in the temperature range of 700 to 725 °C is not significant. The recovery remains close to complete over a wide range of nitrogen additions once the optimum reduction temperature is reached. Once more, for nickel and cobalt there are only small improvements in the metal recoveries at these reduction temperatures. As observed for reduced pressure, the greatest influence of nitrogen occurs at intermediate temperatures where the reduction reactions are close to equilibrium. However, for iron there is a significant increase in the iron recovery with increasing nitrogen, as observed above for the case of reduced atmospheric pressure. Nevertheless, as mentioned previously, this may not be an appealing outcome as the metal alloy grade decreases. Therefore, nitrogen additions provide a thermodynamic benefit for the recovery of the metals by promoting the forward reduction reactions. However, they also enhance iron reduction, which decreases the overall selectivity of Stage I. As a result, the benefit of nitrogen depends on the desired balance between metal recovery and alloy grade.

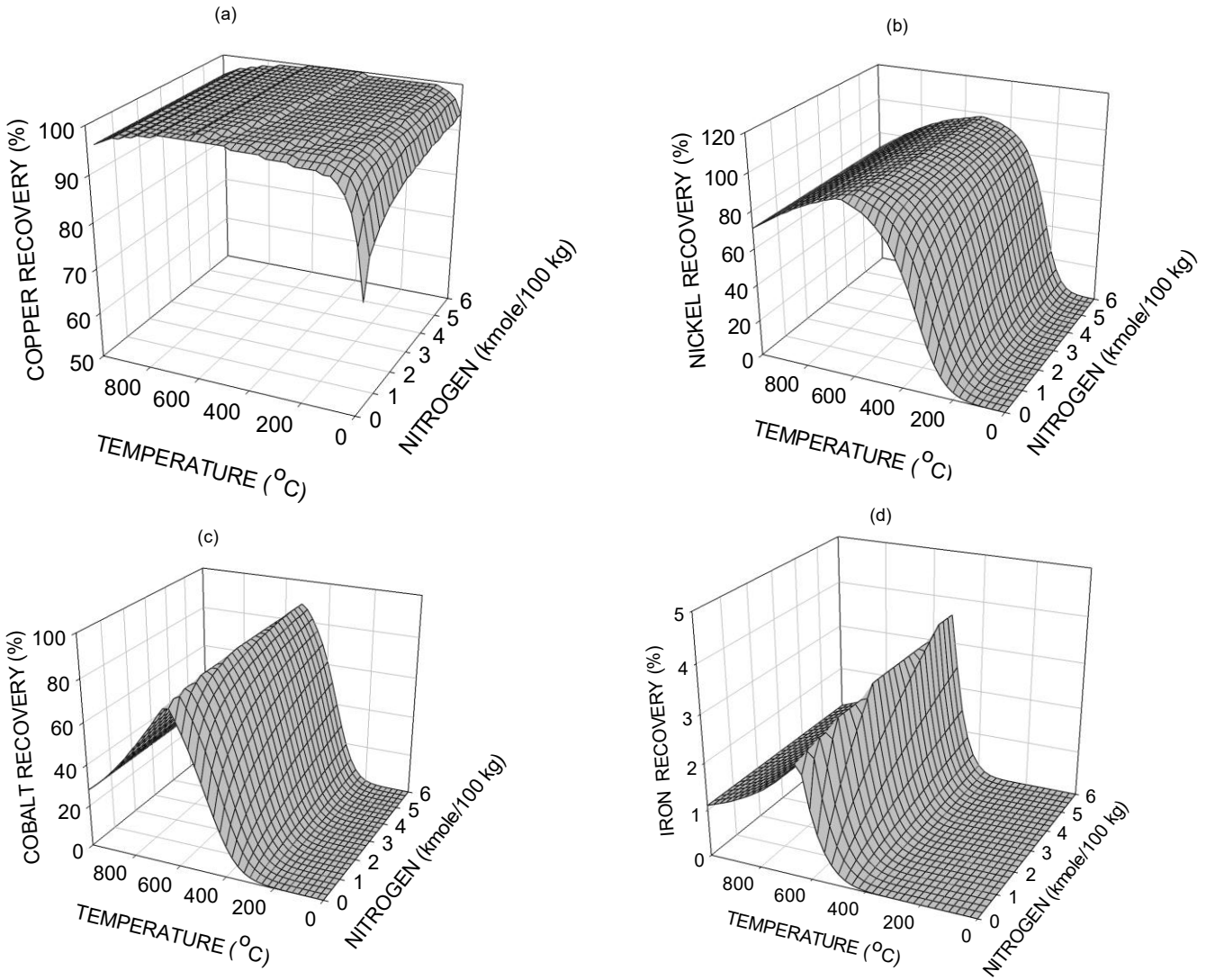


Figure 10 (a) Copper, (b) nickel, (c) cobalt and (d) iron recoveries in Alloy I as a function of temperature and nitrogen additions for a carbon addition of 0.25 kmole/100kg.

The chemical and mineralogical compositions of polymetallic nodules vary both between different regions of the CCZ and among individual growth layers within a nodule [37].The influence of nodules composition was investigated by varying the amounts of the gangue oxides including silica (SiO_2), lime (CaO), alumina (Al_2O_3) and magnesia (MgO). In addition, the effect of iron oxide (Fe_2O_3) was studied. Figures 11(a), (b), (c), (d) and (e) show the effect of the amount of each oxide added on the equilibrium amounts of copper, nickel, cobalt and iron. The carbon addition was 0.25 kmole C/100 kg and the temperature was 700 °C. The importance of iron oxide content is supported by previous thermodynamic and experimental work showing that adjustment of the Mn/Fe ratio through iron oxide addition significantly influences slag formation, liquidus temperature, alloy aggregation and slag–alloy separation [36].

Generally, the addition of each oxide resulted in a decrease in the equilibrium amount of each metal, with the magnitude of the decrease varying for the different oxides and the amount added. For silica, increasing SiO_2 additions result in increasing amounts of silicates. The amounts of copper, nickel and cobalt decreased only slightly at high SiO_2 additions, but there was a significant decrease in the amount of iron. The additional SiO_2 preferentially suppresses iron reduction while having only a limited influence on the recovery of the critical metals. For lime, the amounts of calcium silicates increased, and the decreases in the metals were more significant than for SiO_2 but occurred only at high lime additions. Again, the decrease in iron was more pronounced. The formation of calcium silicates consumes species that would otherwise participate in the reduction reactions. For alumina, aluminosilicates formed in increasing amounts, and the decreases in metal recoveries are essentially continuous but small. However, they become more substantial at high additions. Therefore, alumina has only a minor influence on the equilibrium recovery of the metals within the composition range investigated. In the case of magnesia, increasing amounts of magnesium silicates form and the decreases are relatively small except, once more, for iron. As observed for SiO_2 and lime, iron is affected to a much greater extent than copper, nickel and cobalt.

On the other hand, the addition of iron oxide results in significant decreases in the amounts of nickel and cobalt even at low additions, with decreases in the amount of copper at high additions. Also, the amount of metallic iron decreases. Iron oxide therefore has the greatest influence on the equilibrium composition of Alloy I. Increasing iron oxide additions produce more oxidizing conditions through the conversion of hematite to magnetite and wüstite, thereby introducing additional oxygen into the system and increasing the carbon required for reduction. Consequently, increasing iron oxide additions progressively suppress the reduction of the metals, particularly nickel and cobalt, under the selected operating conditions. The major gangue oxides have only minor effects on the recovery of the metals, whereas iron oxide has a much greater influence because it increases the oxygen potential of the system.

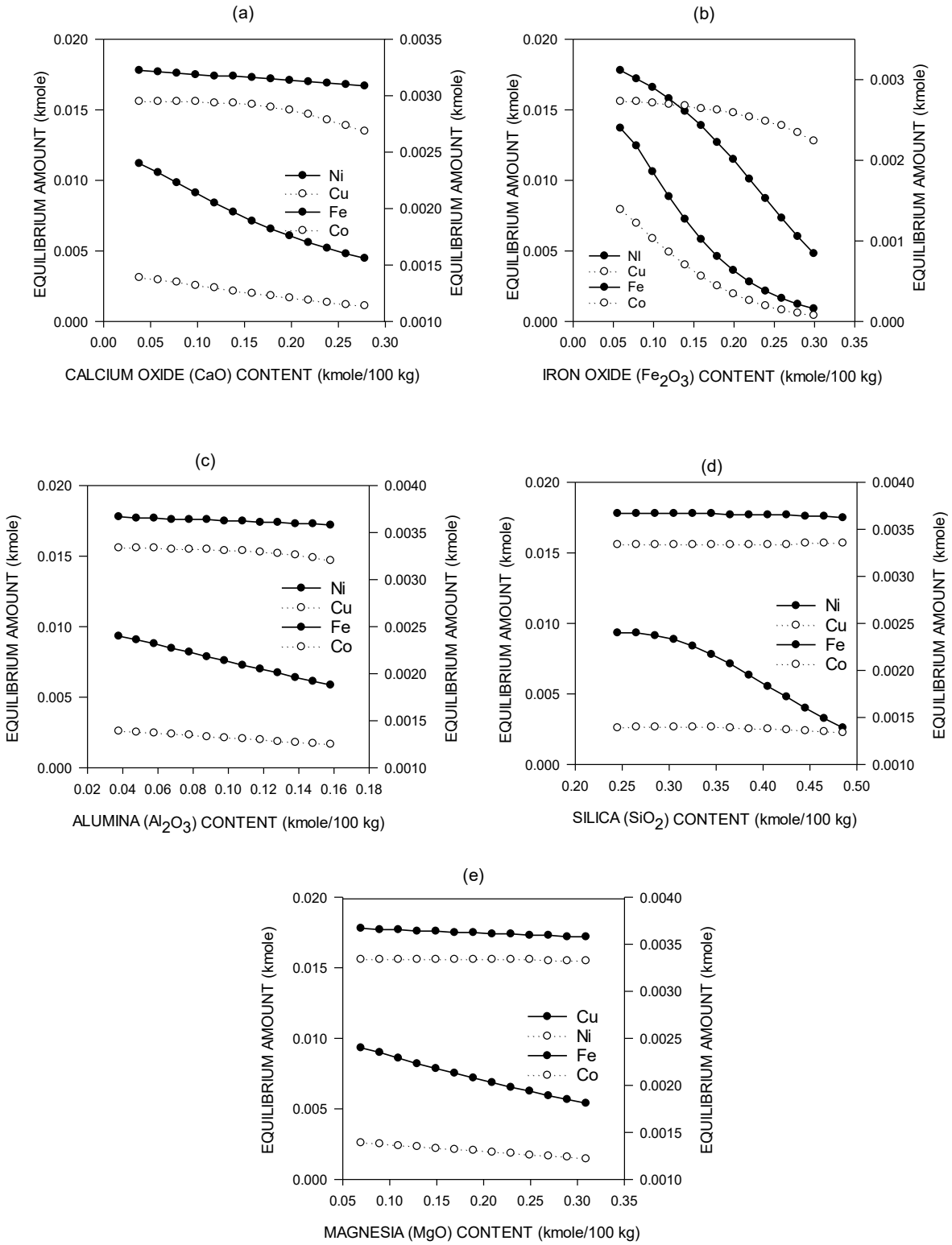


Figure 11 Equilibrium amounts of copper, nickel, cobalt, and iron in Alloy I as a function of (a) lime, (b) hematite, (c) alumina, (d) silica, and (e) magnesia contents for a carbon addition of 0.25 kmole/100 kg at 700 °C. Left axis: Ni and Cu; right axis: Fe and Co.

4.3 Comparison with Experimental Observations

The thermodynamic predictions were compared with published carbothermic reduction and smelting studies of polymetallic nodules. Because these investigations employed different feed compositions, reductants, fluxes and operating conditions, direct quantitative agreement is not expected. The comparison is therefore primarily qualitative, although selected quantitative similarities in metal recoveries are also highlighted in Table 5. Kohga et al. and Zhao et al. reported preferential recovery of Cu, Ni and Co with limited manganese reduction, while Friedmann et al. and Sommerfeld et al. demonstrated the separation of these metals from manganese-rich slags [38,39]. Su et al. and Li et al. further observed that increasing reductant addition promoted greater iron incorporation into the alloy before significant manganese metallization occurred, consistent with the predicted reduction sequence and the calculated loss of selectivity under stronger reducing conditions [24,27]. Differences in the reported temperatures, alloy compositions and metal recoveries are expected because the equilibrium calculations neglect kinetic effects, reaction time, particle size, slag chemistry, reductant–oxide contact and metal coalescence. Nevertheless, the experimental observations consistently support the thermodynamically predicted order of reduction and the existence of a selective operating window in which Cu, Ni and Co are preferentially recovered while manganese remains predominantly in the oxide phase.

Table 5 Comparison of thermodynamic predictions with experimental results for polymetallic nodule reduction.

Experimental conditions and observations	**Present thermodynamic prediction**	Comparison	Ref
• 1250 °C; Mn/Fe = 1.6; C/O = 1.0 • Ni 95.7%, Co 94.6%, Cu 95.1% • Mn remained low • Increasing carbon increased Fe incorporation	• At 700 °C: Ni 97.5%, Co 86.5%, Cu 99.8% • Negligible Mn metallization • Increasing carbon increases Fe incorporation	• Ni: 95.7 vs 97.5% • Cu: 95.1 vs 99.8% • Same carbon–Fe and Mn-retention trends	[24]
• 1100 °C, 2.5 h; 7 wt.% anthracite • Ni 86.48%, Co 86.74%, Cu 83.91%, Fe 91.46%, Mn 5.63%	• At 700 °C: Ni 97.5%, Co 86.5%, Cu 99.8%, Fe 6.9% • Mn remains largely oxidized • Higher temperature/carbon strongly promotes Fe reduction	• Co: 86.74 vs 86.5% • Same low Mn relative to Fe • Higher experimental Fe reflects much stronger reducing conditions	[26]
• 1350 °C • Optimum graphite ≈4 wt.% • Increasing graphite increased Fe reduction and lowered Cu–Ni–Co alloy grade • Excess reductant promoted Mn reduction	• Increasing carbon improves critical-metal reduction but progressively increases Fe reduction • Further carbon promotes Mn reduction and lowers Alloy I selectivity	• Same effect of increasing reductant • Quantitative comparison limited by different carbon basis and smelting conditions	[27]
• 1400 °C; 9.4 wt.% SiO_2 • >90% to nearly 100% Co, Cu, Mo and Ni recovery • >97% Mn remained in slag • Fe recovery ≈80%	• At 700 °C: Cu 99.8%, Ni 97.5%, Co 86.5% • Negligible Mn metallization • Fe reduction increases strongly under more severe conditions	• Similar high Cu–Ni–Co recovery range • Both show strong retention of Mn in the oxide/slag phase	[31]

• 900 °C, 2 h coal reduction; 1400 °C smelting • Recovery: Ni 98.5%, Cu 97.5%, Co 96.8% • Mn to alloy: 0.05% • Excess coal increased Fe and Mn reduction	• At 700 °C: Ni 97.5%, Cu 99.8%, Co 86.5% • Negligible Mn metallization • Higher carbon promotes Fe and eventually Mn reduction	• Ni: 98.5 vs 97.5% • Cu: 97.5 vs 99.8% • Same preferential Cu–Ni–Co/Mn separation	[38]
• Direct smelting of CCZ nodules • Lower MnO/SiO_2 decreased reduction temperature • $MnO/SiO_2 \approx 1–2$ enabled near-complete Mn separation	• Cu, Ni and Co metallize before Mn • Mn remains predominantly oxidized in the Stage I window	• Same selective separation trend • Direct numerical comparison not appropriate because of different feed and flux conditions	[39]

5 CONCLUSIONS

1- A thermodynamic model was developed using HSC Chemistry® 7.1 to investigate the first stage of a proposed two-stage selective carbothermic reduction process for deep-sea polymetallic nodules. The model defined the equilibrium conditions required for the selective recovery of copper, nickel and cobalt while minimizing manganese reduction and limiting iron metallization. Temperature and carbon additions were the two most important factors governing the critical metals recovery. Gangue composition, atmospheric composition and total pressure were also shown to be operating variables. The oxide stabilities could be ranked in the following increasing order: $CuO < NiO < CoO < FeO < MnO < SiO_2 < Al_2O_3 < MgO < CaO$.

2- Copper oxide is the least stable metal oxide and is readily reduced under all conditions considered. Consequently, the optimum operating temperature for selective recovery is governed primarily by the reduction of the more stable nickel and cobalt oxides. Thermodynamic calculations indicate that temperatures of approximately 700 to 800 °C, together with carbon additions of approximately 0.35 to 0.40 kmole C per 100 kg of nodules, provide the optimum operating window. Here both the nickel and cobalt oxides are almost completely reduced, with only limited iron reduction, thereby maintaining excellent selectivity. The hyperstoichiometric carbon requirement arises primarily from the reduction of higher-valency manganese and iron oxides to their lower oxidation states.

3- The composition of the Cu–Ni–Co–Fe alloy depends principally on both the carbon addition and the temperature through their influence on iron reduction. Under typical optimum conditions, the alloy consists predominantly of copper, nickel and cobalt with a limited amount of iron. At the optimum conditions for copper, nickel and cobalt recoveries, increasing either temperature or carbon addition promotes iron metallization, thereby increasing total metal recovery but reducing the critical battery-metal alloy grade. Consequently, the optimum operating conditions represent a compromise between maximizing metal recovery and minimizing iron incorporation into Alloy I.

4- Variations in atmospheric pressure, nitrogen content and nodule composition have only a modest influence on the selective recovery of the critical battery metals. Although reduced pressure and nitrogen additions slightly increase the metal recoveries, their overall effects are limited and are accompanied by increased iron reduction, thereby reducing alloy selectivity. Similarly, gangue oxides have relatively small effects on the copper, nickel and cobalt recoveries but can influence iron recovery through the formation of stable oxide and silicate phases. Among the oxides investigated, variations in iron oxide content had the greatest influence on the equilibrium recovery of the metals.

5- Comparison with published experimental studies showed good qualitative agreement with the predicted reduction behaviour. Experimental results consistently demonstrate preferential recovery of Cu, Ni and Co while manganese remains predominantly in the oxide or slag phase, together with increased iron metallization under stronger reducing conditions. These observations

support the reduction sequence and selectivity trends underlying the Stage I thermodynamic operating window.

6 Acknowledgements

The authors thank the Natural Sciences and Engineering Research Council of Canada (NSERC) for their support of this research.

7 References

[1] C. Rühlemann, S. Knodt, Manganese Nodule Exploration & Exploitation from the Deep Ocean., Journal of Ocean Technology 10 (2015) 13–21.

[2] J.R. Hein, A. Koschinsky, T. Kuhn, Deep-ocean polymetallic nodules as a resource for critical materials, Nature Reviews Earth & Environment 1 (2020) 158–169.

[3] J.L. Mero, Ocean-floor manganese nodules, Economic Geology 57 (1962) 747–767. https://doi.org/10.2113/gsecongeo.57.5.747.

[4] R. Sharma, First nodule to first mine-site: development of deep-sea mineral resources from the Indian Ocean, Current Science 99 (2010) 750–759.

[5] K. Mizell, J.R. Hein, M. Au, A. Gartman, Estimates of Metals Contained in Abyssal Manganese Nodules and Ferromanganese Crusts in the Global Ocean Based on Regional Variations and Genetic Types of Nodules, in: R. Sharma (Ed.), Perspectives on Deep-Sea Mining: Sustainability, Technology, Environmental Policy and Management, Springer International Publishing, Cham, 2022: pp. 53–80. https://doi.org/10.1007/978-3-030-87982-2_3.

[6] R. Sharma, Approach Towards Deep-Sea Mining: Current Status and Future Prospects, in: R. Sharma (Ed.), Perspectives on Deep-Sea Mining: Sustainability, Technology, Environmental Policy and Management, Springer International Publishing, Cham, 2022: pp. 13–51. https://doi.org/10.1007/978-3-030-87982-2_2.

[7] N. Mittal, S. Anand, Reductive Ammonia Leaching Process for Metal Recovery from Polymetallic Nodules: Can There be a Zero Waste Approach?, in: R. Sharma (Ed.), Perspectives on Deep-Sea Mining: Sustainability, Technology, Environmental Policy and Management, Springer International Publishing, Cham, 2022: pp. 263–277. https://doi.org/10.1007/978-3-030-87982-2_10.

[8] Y. Guo, Resolving Critical Raw Materials Supply Crisis With Microwave/RF-Assisted Collection of Seafloor Nodules, IEEE Microwave Magazine 26 (2025) 83–94. https://doi.org/10.1109/MMM.2025.3534600.

[9] M.J. Lindstrom-Parkins, R. Elliott, M. Fong, C. Lee, Review of Polymetallic Sea Nodules and Their Processing Routes, in: Ni-Co 2025, 6th International Symposium on Nickel and Cobalt, Springer Nature Switzerland, Cham, 2025: pp. 779–795. https://doi.org/10.1007/978-3-032-00167-2_59.

[10] N. Birkner, A. Navrotsky, Thermodynamics of manganese oxides: Sodium, potassium, and calcium birnessite and cryptomelane, Proceedings of the National Academy of Sciences 114 (2017) E1046–E1053. https://doi.org/10.1073/pnas.1620427114.

[11] J.E. Post, P.J. Heaney, J. Hanson, Synchrotron X-ray diffraction study of the structure and dehydration behavior of todorokite, American Mineralogist 88 (2003) 142–150. https://doi.org/10.2138/am-2003-0117.

[12] C. Duhayon, S. Boel, Comparative Advantages of the Mineral Processing of Deep-Sea Polymetallic Nodules over Terrestrial Ores, in: R. Sharma (Ed.), Perspectives on Deep-Sea Mining: Sustainability, Technology, Environmental Policy and Management, Springer International Publishing, Cham, 2022: pp. 199–217. https://doi.org/10.1007/978-3-030-87982-2_8.

[13] J. Kim, K.D. Kwon, Tunnel cation and water structures of todorokite: Insights into metal partitioning and isotopic fractionation, Geochimica et Cosmochimica Acta 333 (2022) 153–165. https://doi.org/10.1016/j.gca.2022.07.008.

[14] H. Song, J. Liu, G. Cheng, X. Xue, Microwave-enhanced selective extraction of deep-sea polymetallic nodules, Minerals Engineering 245 (2026) 110387. https://doi.org/10.1016/j.mineng.2026.110387.

[15] A.V. Wegorzewski, M. Köpcke, T. Kuhn, M.A. Sitnikova, H. Wotruba, Thermal Pre-Treatment of Polymetallic Nodules to Create Metal (Ni, Cu, Co)-Rich Individual Particles for Further Processing, Minerals 8 (2018) 523. https://doi.org/10.3390/min8110523.

[16] J. Li, Y. Hu, L. Yue, L. Zeng, S. Wu, M. Wang, W. Guan, Z. Cao, Q. Li, G. Zhang, Recovery of critical battery metals from cobalt-rich deep-sea polymetallic nodules: Selective carbothermal reduction based on kinetics, Journal of Environmental Chemical Engineering 12 (2024) 111631. https://doi.org/10.1016/j.jece.2023.111631.

[17] J. Ju, Y. Feng, H. Li, Z. Xue, R. Ma, Y. Li, Research advances, challenges and perspectives for recovering valuable metals from deep-sea ferromanganese minerals: A comprehensive review, Separation and Purification Technology 315 (2023) 123626. https://doi.org/10.1016/j.seppur.2023.123626.

[18] K.N. Han, D.W. Fuerstenau, Acid leaching of ocean manganese nodules at elevated temperatures, International Journal of Mineral Processing 2 (1975) 163–171. https://doi.org/10.1016/0301-7516(75)90019-8.

[19] A.J. Monhemius, The extractive metallurgy of deep-sea manganese nodules, in: Topics in Non-Ferrous Extractive Metallurgy, SCI London, 1980: pp. 42–69.

[20] D. Dreisinger, N. Verbaan, M. Canizares, The Demonstration of the Cuprion Process for Recovery of Nickel, Cobalt, Copper, and Manganese from Seabed Nodules, in: Proceedings of the 61st Conference of Metallurgists, COM 2022, Springer International Publishing, Cham, 2023: pp. 753–772. https://doi.org/10.1007/978-3-031-17425-4_86.

[21] N. Verbaan, M. Johnson, Revisiting Pressure Acid Leaching of Seabed Polymetallic Nodules, in: Metallurgy and Materials Society of CIM (Ed.), Proceedings of the 63rd Conference of Metallurgists, COM 2024, Springer Nature Switzerland, Cham, 2025: pp. 1235–1242. https://doi.org/10.1007/978-3-031-67398-6_208.

[22] M.N. Boulby, K. Bradley, J.R. Donald, Production of Battery-Grade Sulfates from Deep-Sea Polymetallic Nodules, in: Metallurgy and Materials Society of CIM (Ed.), Proceedings of the 63rd Conference of Metallurgists, COM 2024, Springer Nature Switzerland, Cham, 2025: pp. 1265–1275. https://doi.org/10.1007/978-3-031-67398-6_211.

[23] O.K. Brustad, J. Låstad, A. Hoseinpur, J. Safarian, Characterization, Calcination and Pre-Reduction of Polymetallic Manganese Nodules by Hydrogen and Methane, Metals 12 (2022) 2013. https://doi.org/10.3390/met12122013.

[24] F. Li, S. Xu, J. Qiu, Z. Chen, W. Du, D. Ju, K. Xie, Optimization of Gas–Solid Co-Reduction Conditions for Deep-Sea Polymetallic Nodules, JOM 75 (2023) 5718–5728. https://doi.org/10.1007/s11837-023-06181-y.

[25] U. Manzoor, T. Lüttke, D. Raabe, I.R. Souza Filho, Low-waste, single-step, sustainable extraction of critical metals from deep-sea polymetallic nodules, Science Advances 11 (2025) eaea1223. https://doi.org/10.1126/sciadv.aea1223.

[26] F. Zhao, X. Jiang, S. Wang, L. Feng, D. Li, The Recovery of Valuable Metals from Ocean Polymetallic Nodules Using Solid-State Metalized Reduction Technology, Minerals 10 (2020) 20. https://doi.org/10.3390/min10010020.

[27] K. Su, X. Ma, J. Parianos, B. Zhao, Thermodynamic and Experimental Study on Efficient Extraction of Valuable Metals from Polymetallic Nodules, Minerals 10 (2020) 360. https://doi.org/10.3390/min10040360.

[28] C.A. Pickles, O. Marzoughi, Thermodynamic modelling of spodumene decrepitation, Mineral Processing and Extractive Metallurgy 131 (2022) 130–144. https://doi.org/10.1080/25726641.2020.1827675.

[29] C.A. Pickles, O. Marzoughi, Thermodynamic modelling of decomposition processes in the Mn-O and Mn-O-H systems, Canadian Metallurgical Quarterly 62 (2023) 151–170. https://doi.org/10.1080/00084433.2022.2060602.

[30] O. Marzoughi, C.A. Pickles, L. Tafaghodi, Thermodynamic Analysis of the Selective Solid-State Reduction of Electric Arc Furnace Dust by Methane, in: Cross-Cutting Symposia, Springer Nature Switzerland, Cham, 2025: pp. 345–349. https://doi.org/10.1007/978-3-032-00182-5_37.

[31] M. Sommerfeld, D. Friedmann, T. Kuhn, B. Friedrich, "Zero-Waste": A Sustainable Approach on Pyrometallurgical Processing of Manganese Nodule Slags, Minerals 8 (2018) 544. https://doi.org/10.3390/min8120544.

[32] A. Roine, J. Mansikka-aho, P. Björklund, J. KENTALA, T. Talonen, Outokumpu HSC Chemistry, Chemical reaction and equilibrium software with extensive thermochemical database, Finland Outokumpu Research Oy (2006).

[33] O. Marzoughi, J. Forster, J. Donald, C.A. Pickles, Microwave dewatering of deep-sea polymetallic nodules: Bench-scale and pilot-scale studies, Minerals Engineering 235 (2026) 109879. https://doi.org/10.1016/j.mineng.2025.109879.

[34] O. Marzoughi, R. Verge, S. Annan, R.M. Hutcheon, J. Donald, C.A. Pickles, Characterization, permittivities and drying kinetics during microwave dewatering of deep-sea polymetallic nodules, Chemical Engineering Journal Advances 26 (2026) 101102. https://doi.org/10.1016/j.ceja.2026.101102.

[35] R.A. Rapp, F. Maak, Thermodynamic properties of solid copper-nickel alloys, Acta Metallurgica 10 (1962) 63–69. https://doi.org/10.1016/0001-6160(62)90187-6.

[36] F. Li, S. Xu, D. Zhou, D. Ju, W. Du, H. Wang, Optimized Conditions for Extracting Fe–Ni–Co–Cu Alloy from Polymetallic Nodules, J. Sustain. Metall. 9 (2023) 1363–1377. https://doi.org/10.1007/s40831-023-00732-y.

[37] J. Li, Y. Jin, H. Wang, K. Yang, Z. Zhu, X. Meng, X. Li, In-situ analysis of polymetallic nodules from the clarion-Clipperton zone, Pacific Ocean: implication for controlling on chemical composition variability, Front. Mar. Sci. 11 (2024). https://doi.org/10.3389/fmars.2024.1489184.

[38] T. Kohga, M. Imamura, J. Takahashi, N. Tanaka, T. Nishizawa, Recovering iron, manganese, copper, cobalt, and high-purity nickel from sea nodules, JOM 47 (1995) 40–43. https://doi.org/10.1007/BF03221339.

[39] D. Friedmann, A.K. Pophanken, B. Friedrich, Pyrometallurgical Treatment of High Manganese Containing Deep Sea Nodules, J. Sustain. Metall. 3 (2017) 219–229. https://doi.org/10.1007/s40831-016-0070-8.